TÜBİTAK

Turkish Journal of Physics

http://journals.tubitak.gov.tr/physics/

Research Article

Turk J Phys
(2017) 41: 81 – 89
© TÜBİTAK
doi:10.3906/fiz-1607-9

Determination of height profile from a two-dimensional fringe signal using a two-dimensional continuous wavelet transform

Özlem KOCAHAN*
Department of Physics, Faculty of Arts and Sciences, Namık Kemal University, Tekirdağ, Turkey

Received: 14.07.2016 • **Accepted/Published Online:** 20.10.2016 • **Final Version:** 02.03.2017

Abstract: The main objective of this study was 3-dimensional (3D) profile measurements with standard fringe projection, consisting of a CCD and a projector. For obtaining height information of objects pixel by pixel, phases have to be calculated from the images taken by the fringe projection technique. In this study, the 2-dimensional continuous wavelet transform (2D CWT) phase method was used for phase extraction. 1D and 2D CWT analyses of noisy images were compared in simulations performed for a 2-dimensional fringe signal by introducing the carrier frequencies in two spatial directions, x and y. Profile measurement of an object was made experimentally by cross optical axis geometry. Images, using fringes with two carrier frequencies, taken from this setup were analyzed with 2D CWT and 3D profiles of objects were obtained. Numerical simulations and actual experiments were carried out to show the validity of this technique for finding phase distributions from noisy images.

Key words: Continuous wavelet transform, wavelet transform profilometry, fringe projection techniques, phase calculation, fringe pattern

1. Introduction

Nowadays, there is extensive research on optical measuring systems, which stand out due to the following features: reliability, high precision, and quick and easy applicability in a digital environment. To determine the height profile of objects by the fringe projection technique, a practical measuring system can be designed with high precision. In 1983, Takeda calculated 3-dimensional (3D) surface profiles from the image taken by sinusoidal fringe pattern projection, with the use of the Fourier transform (Fourier transform profilometry (FTP)) [1]. In the following years, more advanced measurement systems were designed with Morie and sinusoidal fringe projection techniques and surface profile calculation methods experimented by different integral transforms and phase shifting. Over the years, the importance of fringe projection profilometry has increased in the field of optical measurement and it has been applied in many areas such as biomedical applications like oral and dental measurements, histology, and cell biology, as well as many areas of industry, e.g., quality control, surface measurement, and characterization of microelectromechanical components [2–5].

3D surface measurement with the fringe projection technique (without touching) consists of three main units: projection unit, image recording unit, and image analysis unit [3]. As an optical measurement, in this method, the fringe pattern is projected onto the sample at first and then the image from this setup is recorded. The fringe pattern is deformed because of the objects' height. Height information within this image is obtained from the phase term in the Fourier transform [2]. The deformed image is analyzed with an algorithm generated

*Correspondence: okocahan@nku.edu.tr

by Fourier or one of the other integral transforms and in this way phase information is retrieved. Then this phase information is converted to height from the geometry of the setup. After determining the height of each point on the surface (pixel by pixel) from the reference plane, these are brought together to provide the 3D profile of the object [1,3].

In the present study, a two-dimensional (2D) continuous wavelet transform (CWT) was used for the calculation of phase from a fringe pattern by introducing the carrier frequencies in two spatial directions, x and y, for the first time. Since 1983, the Fourier transform has been as the most commonly used phase distribution calculation technique according to the literature. On the other hand, CWT was applied as a simulation for the fringe projection technique for the first time in 1999 and it has been frequently used since [6]. In particular, noisy images, taken from a fringe pattern with one carrier frequency, are analyzed successively with 2D CWT [7,8]. Noise is an expected feature for micrometer range profilometry [9–11]. The aim of the present study was to examine the validity of this method for obtaining more precise results from noisy images taken from a fringe pattern with two carrier frequency by 2D CWT. To achieve this goal, a simulation and experiments were carried out.

2. CWT method for phase calculation

2.1. 1D CWT method

Consider the following 2D fringe signal:

$$h(x) = I_0(x)\left[1 + V(x)\cos\left(2\pi f_0 x + \varphi(x)\right)\right], \tag{1}$$

where $I_0(x)$ is the background intensity, $V(x)$ is the visibility of the fringe, $\varphi(x)$ is the height-modulated phase of the fringe, and f_0 is the spatial carrier frequency that must satisfy the following condition to recover the phase [1]:

$$2\pi f_0 > \left|\frac{d\varphi}{dx}\right|_{max} \tag{2}$$

The 1D wavelet transform of the fringe signal is defined by [12]

$$\begin{aligned} CWT(a,b) &= \frac{1}{a^{1/2}}\int_{-\infty}^{\infty} h(x)\Psi^*\left(\frac{x-b}{a}\right)dx \\ &= a^{1/2}\int_{-\infty}^{\infty}\hat{\Psi}^*(a\alpha)\hat{H}(\alpha)\,exp(ib\alpha)d\alpha \end{aligned} \tag{3}$$

Each wavelet is obtained by scaling a mother wavelet $\Psi\left(\frac{x-b}{a}\right)$ with scaling parameter $a > 0$ and translating it by b. Ψ^* shows the complex conjugate of the mother wavelet. The second form of Eq. (3) allows the use of a fast Fourier transform algorithm and results in much faster calculations, where $a^{1/2}\hat{\Psi}(a\alpha)$ and $\hat{H}(\alpha)$ are the Fourier transforms of $a^{-1/2}\Psi\left(\frac{x-b}{a}\right)$ and $h(x)$, respectively [12,13].

The Morlet wavelet, which is a plane wave modulated by a Gaussian, is defined as

$$\Psi(x) = \pi^{1/4}\exp(icx)\exp\left(-\frac{x^2}{2}\right) \tag{4}$$

and its Fourier transform has the form

$$\hat{\Psi}(\alpha) = \frac{\sqrt{2\pi}}{\sqrt[4]{\pi}} \exp\left[-\frac{(\alpha - c)^2}{2}\right], \tag{5}$$

where c is a fixed spatial frequency and is chosen to be about 5 or 6 to satisfy the admissibility condition [13].

Based on the localization property [14], the phase of the fringe can be approximated by $\varphi(x) \cong \varphi(b) + (x-b)\varphi'(b) + \ldots$. Furthermore, assuming a slow variation of $I_0(x)$ and $V(x)$, the Fourier transform of the fringe signal is evaluated as

$$\begin{aligned} \hat{H}(\alpha) &= I_0(b)\pi 2\delta(\alpha) + I_0(b)\pi V(b)\delta\left(\alpha - f_0 - \frac{\varphi'(b)}{2\pi}\right)\exp\left[i\left(\varphi(b) - b\varphi'(b)\right)\right] \\ &\quad + I_0(b)\pi V(b)\delta\left(\alpha + f_0 + \frac{\varphi'(b)}{2\pi}\right)\exp\left[-i\left(\varphi(b) - b\varphi'(b)\right)\right]. \end{aligned} \tag{6}$$

Then, substituting Eqs. (5) and (6) into Eq. (3) and noting that $\hat{\Psi}(a\alpha) = 0$ for $\alpha \leq 0$, the Morlet wavelet transform is obtained as

$$CWT(a,b) = I_0(b)V(b)\pi^{5/4}\sqrt{2a}\exp\left\{\frac{\left[a\left(2\pi f_0 + \varphi'(b)\right) - c^2\right]}{2}\right\}\exp\left\{i\left[\varphi(b) + 2\pi f_0 b\right]\right\} \tag{7}$$

2.2. 2D CWT method

Consider the following 2D fringe signal:

$$h(x,y) = I_0(x,y)\left[1 + V(x,y)\cos\left(2\pi f_0 x + 2\pi f_0 y + \varphi(x,y)\right)\right] \tag{8}$$

The 2D CWT of the fringe signal is defined by

$$CWT(a,b,\theta) = \frac{1}{a}\int_{-\infty}^{\infty}\Psi^*\left(\frac{x-b_x}{a}, \frac{y-b_y}{a}, r_{-\theta}\right)h(x,y)\,dxdy, \tag{9}$$

where $\Psi\left(\frac{x-b_x}{a}, \frac{y-b_y}{a}, r_{-\theta}\right)$ is the analyzing wavelet with scale parameter $a(a>0)$, and translation parameter b. $r_{-\theta}$ is the rotation matrix of size 2×2, which acts on (x,y) as [7,15]

$$r_{-\theta}(x,y) = (x\cos\theta + y\sin\theta, -x\sin\theta + ycos\theta) \tag{10}$$

and θ is a rotation angle. Eq. (9) can be written in the Fourier domain by using the convolution theorem to decrease the calculation time [12,15,16]

$$CWT(a,b,\theta) = a\int_{-\infty}^{\infty}\int_{-\infty}^{\infty}\hat{\Psi}^*\left(ar_{-\theta}\alpha_x, ar_{-\theta}\alpha_y\right)\hat{H}(\alpha_x,\alpha_y) \tag{11}$$

$\hat{H}(\alpha_x,\alpha_y)$ and $\hat{\Psi}\left(ar_{-\theta}\alpha_x, ar_{-\theta}\alpha_y\right)$ are the Fourier transforms of $h(x,y)$and $\frac{1}{\sqrt{a}}\Psi\left(\frac{x-b_x}{a}, \frac{y-b_y}{a}, r_{-\theta}\right)$, respectively.

Mother wavelet selection is an important step for the determination of phase from a projected fringe pattern [17]. In the present study, a 2D Morlet wavelet was chosen, which is defined as [7]

$$\Psi\left(\frac{x-b_x}{a},\frac{y-b_y}{a},r_{-\theta}\right)=\exp\left[ic\frac{(x-b_x)\cos\theta+(y-b_y)\sin\theta}{a}\right]\exp\left[-\frac{(x-b_x)^2+(y-b_y)^2}{2a}\right] \tag{12}$$

and its Fourier transform is

$$\hat{\Psi}\left(ar_{-\theta}\alpha_x,ar_{-\theta}\alpha_y\right)=\exp\left[-\frac{(a\alpha_x-c\cos\theta)^2+(a\alpha_y-c\sin\theta)^2}{2}\right] \tag{13}$$

Based on the localization property of the CWT [14,18], the phase of the fringe can be approximated by $\varphi(x,y)\cong\varphi_b+(x-b_x)\,\varphi'_x+(y-b_y)\,\varphi'_y+\ldots$. Here, $\varphi_b=\varphi(b_x,b_y),\varphi'_x=\partial\varphi(b_x,b_y)/\partial x$ and $\varphi'_y=\partial\varphi(b_x,b_y)/\partial y$. Furthermore, assuming a slow variation of $I_0(x,y)$ and $V_0(x,y)$, the Fourier transform of the fringe signal is evaluated as

$$\hat{H}\left(\alpha_x,\alpha_y\right)=A_1+A_2+A_3 \tag{14}$$

$$A_1=2\pi I_0\left(b_x,b_y\right)\delta\left(\alpha_x,\alpha_y\right)$$

$$A_2=\pi I_0\left(b_x,b_y\right)V\left(b_x,b_y\right)$$

$$\exp\left[i\left(\varphi_b-b_x\varphi_x^{'}-b_y\varphi_y^{'}\right)\right]$$

$$\delta\left(\alpha_x-2\pi f_0-\varphi_x^{'},\,\alpha_y-2\pi f_0-\varphi_y^{'}\right)$$

$$A_3=\pi I_0\left(b_x,b_y\right)V\left(b_x,b_y\right)$$

$$\exp\left[-i\left(\varphi_b-b_x\varphi_x^{'}-b_y\varphi_y^{'}\right)\right]$$

$$\delta\left(\alpha_x+2\pi f_0+\varphi_x^{'},\,\alpha_y+2\pi f_0+\varphi_y^{'}\right)$$

Then, substituting Eqs. (13) and (14) into Eq. (11) and noting that $\hat{\Psi}\left(ar_{-\theta}\alpha_x,ar_{-\theta}\alpha_y\right)=0$ for $\alpha_{x,y}\leq 0$, CWT is evaluated as

$$\begin{aligned}CWT\left(a,b,\theta\right) &= \pi I_0\left(b_x,b_y\right)V\left(b_x,b_y\right)exp\left[i\left(\varphi_b+2\pi f_0b_x+2\pi f_0b_y\right)\right]\\ &\quad\exp\left\{-\frac{1}{2}\left[\left(a2\pi f_0+a\varphi_x^{'}-c\cos\theta\right)^2+\left(a2\pi f_0+a\varphi_y^{'}-c\sin\theta\right)^2\right]\right\}\end{aligned} \tag{15}$$

In the CWT phase method, the wrapped phase distribution is directly acquired from the phase of CWT (Eqs. (7) and (15)) and the unwrapped phase is obtained by using a suitable unwrapping algorithm to correct phase discontinuities [14,19].

3. Simulation and experimental work

As an example, to test the above phase recovery algorithms, the following 2D simulated phase modulation function was used (Figure 1a):

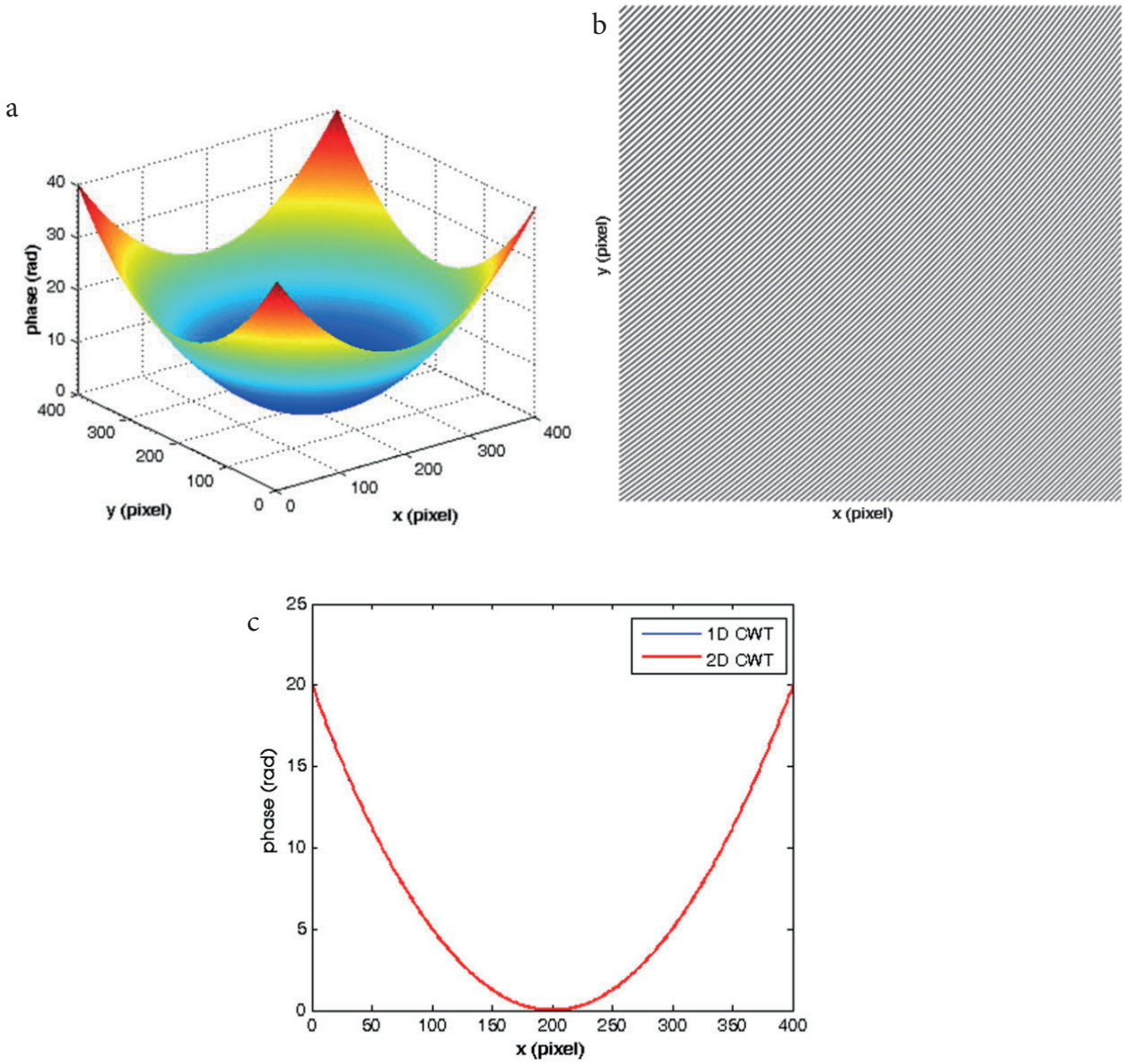

Figure 1. a) Simulated fringe pattern; b) Fringe pattern, with the spatial frequency in the x and y directions, corresponding to test phase; c) Calculated phase values of the simulated fringe pattern for the rows $y = 200$.

$$\varphi(x,y) = 0.0005\left[(x-200)^2 + (y-200)^2\right] \tag{16}$$

The fringe pattern corresponding to this phase function (Figure 1b) was calculated by taking $I_0(x,y) = V(x,y) = 1$ and $f_0 = 0.2$ (1/pixel) in Eq. (1). The simulated phase function and the phases, which were

recovered by applying the 2D and 1D CWT with the Morlet wavelet, are compared in Figure 1c for the line y = 200. The execution time for the 1D CWT analysis was 87.913 s, whereas it was 14.056 seconds for the 2D CWT.

2D CWT has an advantage when noisy images are analyzed [7,8]. To test this, a speckle noise of zero mean with a 0.03 variance was added to the fringe pattern given in Figure 1b, and the ultimate shape is depicted in Figure 2a. The recovered phase distributions, for the line y = 200, by both 1D and 2D CWT are shown in Figure 2b. Phase values obtained from noisy images and simulated phases are compared for four different pixel numbers in Table 1.

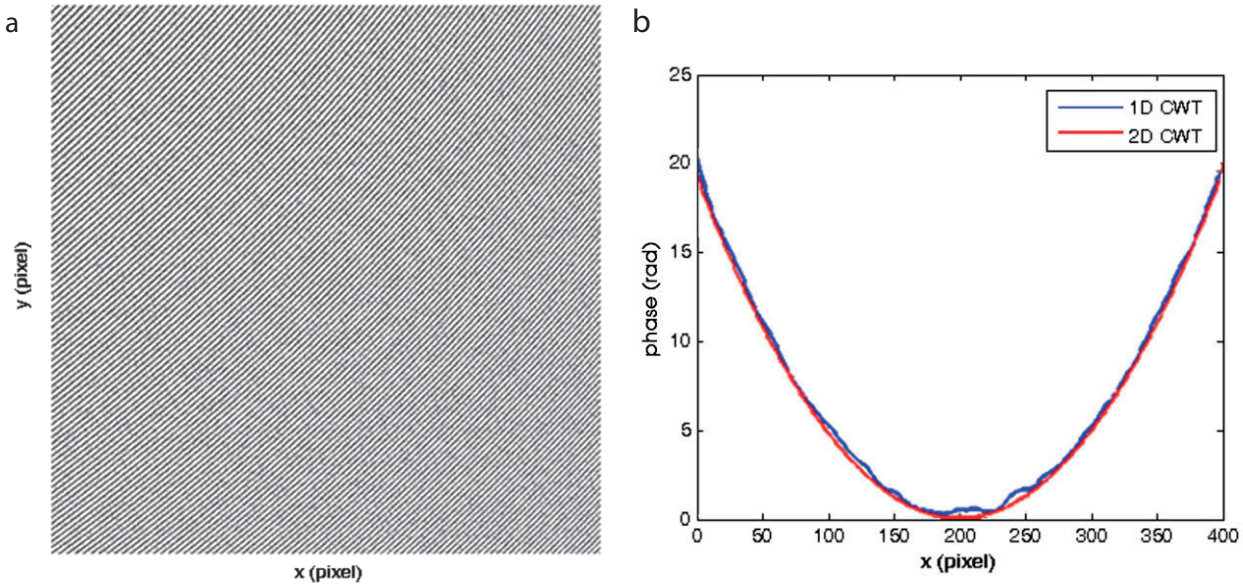

Figure 2. a) Fringe pattern with speckle noise; b) Calculated phase values from the noisy fringe pattern for the rows $y = 200$.

Table 1. Comparison for phase values of simulated noisy signal and the phases calculated from this signal by 1D CWT and 2D CWT are given for four different pixel numbers.

	Phase values (rad)			Phase error (%)	
Pixel Number (X × Y)	1D CWT	2D CWT	Simulated noisy signal	1D CWT	2D CWT
100 × 100	10.459	9.952	10	4.59	0.48
200 × 200	0.189	0.037	0	1.89	0.37
300 × 300	10.533	10.030	10	5.33	0.30
400 × 400	40.792	39.276	40	1.98	1.81

A schematic diagram of the experimental setup using crossed optical axes geometry is presented in Figure 3. The fringe pattern with the carrier frequency in two spatial directions, x and y, given in Eq. (1) was calculated by taking $\varphi(x, y) = 0$. This sinusoidal fringe pattern was projected by a projector (BENQ MP512) with a resolution of 600 × 800 pixel onto a mask mechanically measured as 3.50 cm high around the nose. The distance from the CCD camera (CANON - IXSUS, 10 megapixels) to reference plane, L, was 175 cm; the distance between projector and camera, d, was 14.5 cm, and the period of fringes on the reference plane, p_0, was 0.8 cm. The CCD camera was focused on the center of the reference plane. Firstly, the reference image and then the object image, shown in Figure 4a, were captured and converted into grayscale for analysis.

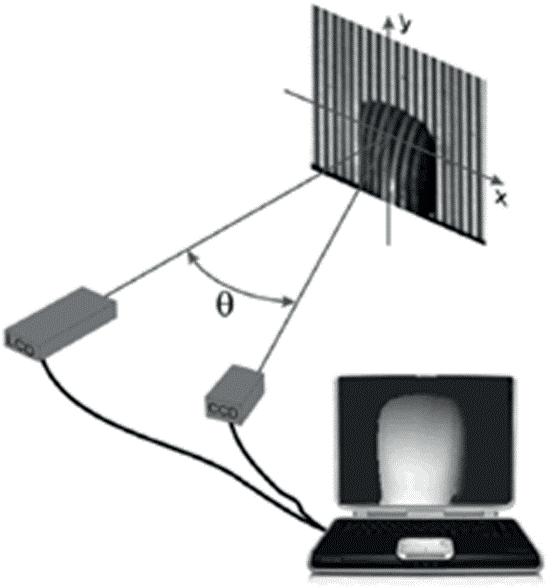

Figure 3. Experimental setup for fringe projection.

In 2D CWT method with the Morlet wavelet, phase distributions of the reference image $\varphi_R(x,y)$ and the object image $\varphi_0(x,y)$ were obtained. Afterwards, the phase distribution of the object $\varphi(x,y) = \varphi_0(x,y) - \varphi_R(x,y)$ was calculated by the 2D CWT phase method. Because the measured object in this work had a smooth surface, the phase as wrapped in the $[-\pi, +\pi]$ range was unwrapped using the unwrap subroutine of MATLAB to correct discontinuities and the correct phase was retrieved. Finally, the height values of the object surface were determined as follows [1]:

$$z(x,y) = \frac{Lp_0\left(\frac{\phi(x,y)}{2\pi}\right)}{\left[p_0\left(\frac{\phi(x,y)}{2\pi}\right) - d\right]}, \tag{17}$$

where z is the surface height. The height profile, obtained from the phase method using 2D CWT is shown in Figure 4b. In Table 2, retrieved height values are compared with a mechanically measured one for four different pixel numbers.

Table 2. Comparison for height values of mask from 2D CWT and mechanical measurement are given for four different pixel numbers.

		Height values (cm)	Height error (%)
Pixel Number (X × Y)	2D CWT	Mechanically measured	
50×50	2.083	2.150	3.116
80×280	3.849	3.950	2.556
200×60	3.329	3.500	4.885
270×300	2.840	3.000	5.333

Furthermore, to test the noise analysis, speckle noise of zero mean with 0.03 variance was added to the images retrieved from the experiment, and the noisy object image is shown in Figure 5a. The calculated height profile from these noisy images by 2D CWT is given in Figure 5b.

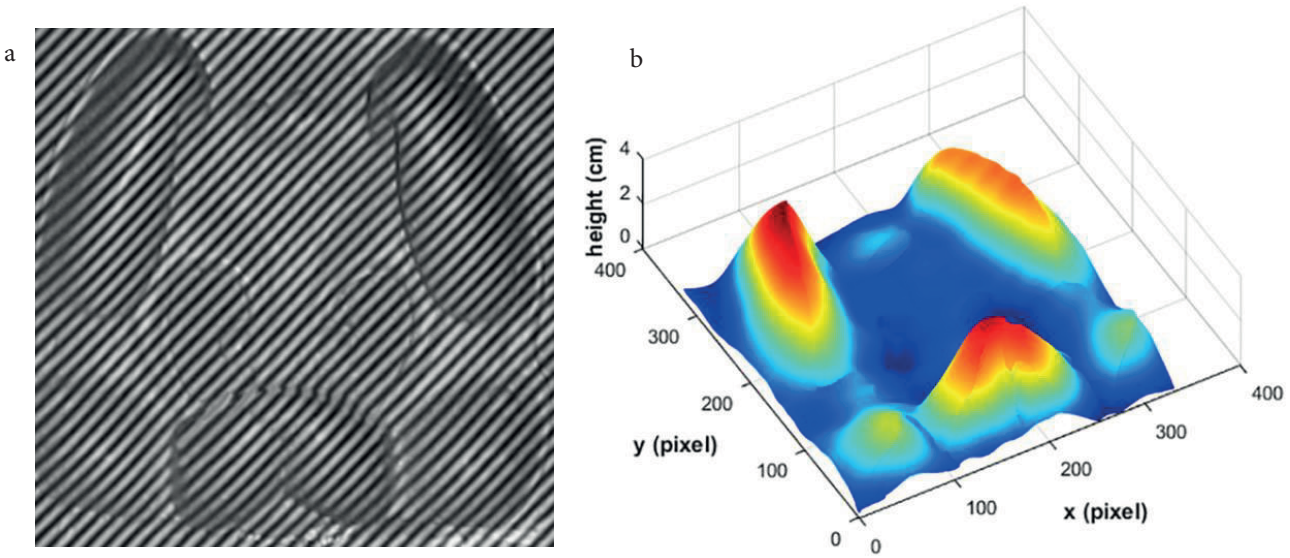

Figure 4. a) Sinusoidal 2D fringe projected image of the mask; b) Recovered height profile of the mask by 2D CWT.

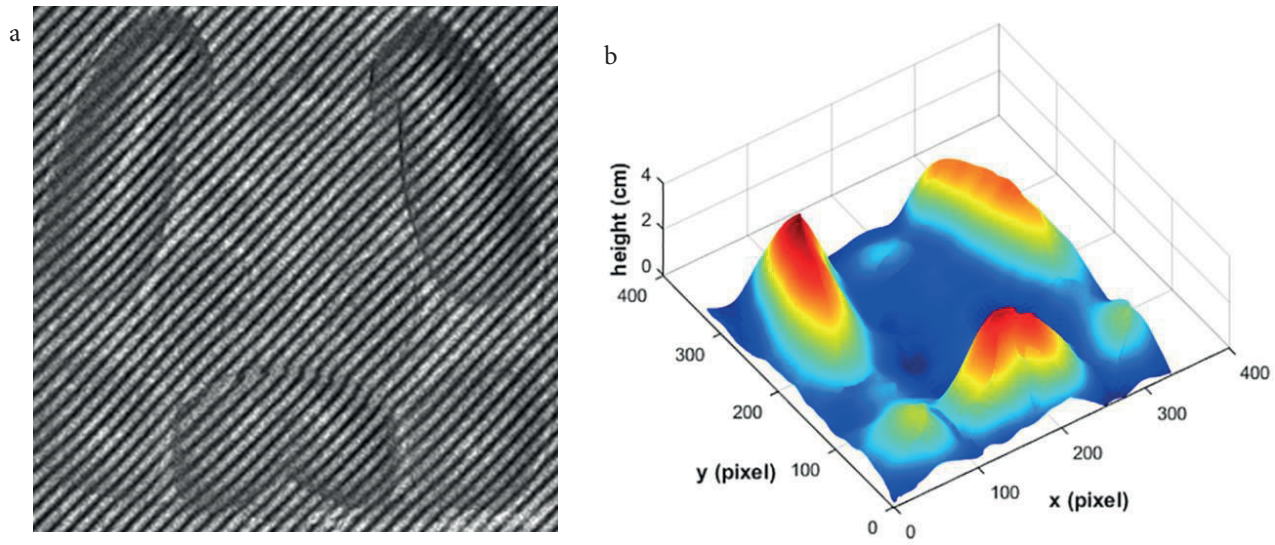

Figure 5. a) Sinusoidal 2D fringe projected image with speckle noise; b) Recovered height profile of the mask from the noisy images by 2D CWT.

4. Conclusion

The 2D CWT of a 2D fringe pattern by introducing the carrier frequencies in two spatial directions, x and y, was used for the first time to recover the height information, according to the literature. The simulation showed 1D CWT is very convenient for the analysis of clean images; in contrast, 2D CWT gives more accurate results in noisy images. Furthermore, this technique has an advantage that the execution time is much shorter than for 1D CWT. Height profiles retrieved by 2D CWT for the clean and noisy images obtained from the experiment are very close to each other. This reveals how appropriate CWT analysis is for such applications.

References

[1] Takeda M, Mutoh K. *Appl. Opt.* **1983**, *22*, 3977.

[2] Su X, Chen W. *Opt. Lasers Eng.* **2001**, *35*, 263-284.

[3] Gorthi SS, Rastogi P. *Opt. Lasers Eng.* **2010**, *48*, 133-140.

[4] Moore CJ, Burton DR, Skydan O, Sharrock PJ, Lalor M. *International Conference on Medical Information Visualisation–BioMedical Visualisation (MedVis'06)* **2006**, 97-102.

[5] Pham HV, Edwards C, Goddard LL, Popescu G. *Appl. Opt.* **2013**, *52*, A97-101.

[6] Watkins LR, Tan SM, Barnes TH. *Opt. Lett.* **1999**, *24*, 905.

[7] Niu H, Quan C, Tay C J. *Opt. Lasers Eng.* **2009**, *47*, 1334-1339.

[8] Gdeisat M, Burton D, Lilley F, Lalor M, Moore C, Rastogi PK, Hack E. *Appl. Opt.* **2010**, *45*, 112-117.

[9] Quan C, He XY, Wang CF, Tay CJ, Shang HM. *Opt. Commun.* **2001**, *189*, 21-29.

[10] Lai C, Hsu I. *Opt. Express* **2007**, *15*, 13949.

[11] Reolon D, Jacquot M, Verrier I, Brun G, Veillas C. *Opt. Express* **2006**, *14*, 128-137.

[12] Meyers SD, Kelly BG, O'Brien JJ. *Mon. Weather Rev.* **1993**, *121*, 2858-2866.

[13] Torrence C, Compo GP. *Bull. Am. Meteorol. Soc.* **1998**, *79*, 61-78.

[14] Dursun A, Özder S, Ecevit FN. *Meas. Sci. Technol.* **2004**, *15*, 1768-1772.

[15] Wang N, Lu C. *J. Atmos. Ocean. Technol.* **2010**, *27*, 652-666.

[16] Arfken GB, Weber HJ. *Mathematical Methods for Physicists*; Academic Press: Boston, MA, USA, 2005.

[17] Addison PS. *The Illustrated Wavelet Transform Handbook*; Bristol, UK: IOP, 2002.

[18] Daubechies I. *IEEE T. Inf. Theory* **1990**, *36*, 961-1005.

[19] Zhang Z, Jing Z, Wang Z, Kuang D. *Opt. Lasers Eng.* **2012**, *50*, 1152-1160.